PAPER

Check for updates

Zero valent iron-electro-Fenton-peroxymonosulfate (ZVI-E-Fenton-PMS) process for industrial wastewater treatment

Song Wang[ab] and Yonggang Zhang [ID] *[ab]

Advanced oxidation processes are frequently applied to a variety of refractory organic wastewater, but rarely is electro-Fenton combined with activated persulfate technology applied to the removal of refractory pollutants. In this work, the electro-Fenton process was combined with zero-valent iron (ZVI) activated peroxymonosulfate (PMS), two advanced oxidation processes based on different radicals, to form the ZVI-E-Fenton-PMS process to treat wastewater, whose main advantages are the generation of more reactive oxygen species and the reduction of oxidant cost to achieve rapid removal of pollutants. This process can not only produce H_2O_2 and activate PMS at the cathode, but also reduce Fe(III) to realize the sustainable Fe(III)/Fe(II) redox cycle. The main reactive oxygen species in the ZVI-E-Fenton-PMS process were found to be ${}^{\bullet}OH$, $SO_4^{\bullet-}$ and ${}^1O_2$ by radical scavenging experiments and electron paramagnetic resonance (EPR), and the relative contributions of the three reactive oxygen species for the degradation of MB were estimated to 30.77%, 39.62% and 15.38%, respectively. Then, by calculating the ratio of the relative contributions of each component to the removal of pollutants at different PMS doses, it was found that the synergistic effect of the process was better when the proportion of ${}^{\bullet}OH$ in the oxidation of reactive oxygen species (ROS) was higher and the proportion of non-ROS oxidation increased year-on-year. This study provides a new perspective on the combination of different advanced oxidation processes and reveals the advantages and potential of this process for application.

1 Introduction

With the rapid development of industrialization and urbanization, the resulting ecological and environmental problems are becoming more and more serious, and the water pollution problem is especially serious, and its damage to the natural environment and the threat to human health mean the treatment of various types of wastewater has become a very important research topic in the environmental field. Industrial wastewater such as printing and dyeing wastewater, pharmaceutical wastewater, electroplating wastewater, *etc.* has been a major research point in the field of water environment due to its high concentration of organic pollutants, not being easy to degrade, with strong toxicity, poor biodegradability and environmental persistence or being teratogenic and carcinogenic to the human body.[1,2] The treatment of industrial wastewater has been a major research point in the field of water environment, and the commonly used methods for treating industrial organic wastewater are mainly biological, physical and chemical processes. Due to the characteristics of industrial wastewater, it

is difficult for traditional wastewater treatment technologies to degrade such pollutants.[3] Many chemical and physical methods have been studied to remove industrial wastewater, such as adsorption, membrane separation and advanced oxidation processes (AOPs).[4–6]

AOPs are commonly used for the treatment of refractory organic wastewater, because they can directly mineralize organic pollutants by generating reactive oxygen species (ROS) in solution or improve the biodegradability of complex pollutants by oxidizing them into small molecules. It has a good application prospect, and they are of great interest in the treatment of refractory organic pollutants.[7–9] AOPs are mainly divided into hydroxyl radical-based advanced oxidation processes (HR-AOPs) and sulfate radical-based advanced oxidation processes (SR-AOPs).[10] HR-AOPs such as Fenton oxidation process, photocatalytic oxidation process, electrochemical oxidation process,[11–14] *etc.* have great potential in degrading difficult biodegradation and persistent organic compounds in wastewater, groundwater, surface water and soil, mainly using the generated high reaction rate and non-selective ${}^{\bullet}OH$ to purify wastewater. Among the HR-AOPs, Fenton, especially electro-Fenton (E-Fenton), has been widely used in the treatment of refractory organic pollutants, which E-Fenton is based on the traditional Fenton oxidation with electrochemical *in situ* generation of H_2O_2, which effectively improves a series of

*a*State Key Laboratory of Separation Membranes and Membrane Processes, Tiangong University, Tianjin 300387, China. E-mail: zhangyonggang1895@163.com

*b*School of Environmental Science and Engineering, Tiangong University, Tianjin 300387, China

problems of transportation, storage and addition of H_2O_2 in the traditional Fenton, and becomes an electrochemical advanced oxidation process (EAOP) for effective degradation of organic pollutants that have received wide attention. E-Fenton process is *in situ* generation of H_2O_2 by an oxygen reduction reaction (ORR) at the cathode in the electrochemical process, and the Fenton reaction with the added Fe^{2+} to form $^{\cdot}OH$ (eqn (1) and (2)).[15,16] To prevent sludge generation (precipitation of Fe^{3+}), researchers often use non-homogeneous catalysts such as zero-valent iron (ZVI), hematite and magnetite (Fe_3O_4), which are low cost, easy to separate and environmentally friendly, instead of Fe^{2+}.[17] It solves the problem of sludge generation while facilitating the recovery and secondary use of the catalyst.

$$O_2 + 2H^+ + 2e^- \rightarrow H_2O_2 \quad (1)$$

$$Fe^{2+} + H_2O_2 + H^+ \rightarrow {}^{\cdot}OH + Fe^{3+} + H_2O \quad (2)$$
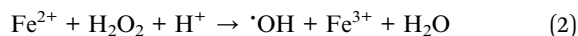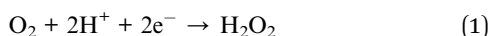
In recent years, SR-AOPs have emerged as promising AOPs that can produce $SO_4^{\cdot-}$ by cleaving the peroxide bonds of peroxymonosulfate (PMS) and peroxydisulfate (PDS),[18] which possess similar or higher redox potentials than $SO_4^{\cdot-}$ (2.5–3.1 V for $SO_4^{\cdot-}$ *vs.* 2.8 V for $^{\cdot}OH$)[19] and longer half-life (30–40 μs for $SO_4^{\cdot-}$ *vs.* 20 ns for $^{\cdot}OH$),[20] which can theoretically degrade organic pollutants more efficiently than $^{\cdot}OH$.[21–23] Among them, PMS is an asymmetric peroxide whose unique structure makes it a common oxidant for $SO_4^{\cdot-}$ generation.[24] It can be activated by different mechanisms, including energy or electron transfer, and thus can generate $SO_4^{\cdot-}$ by various activation methods such as UV, transition metal ions, electrochemistry, carbon catalysts, MOFs,[25–27] *etc.* Moreover, other ROS including free radicals such as superoxide radicals ($^{\cdot}O_2^-$), hydrogen peroxide radicals ($^{\cdot}HO_2$), hydroxyl radicals ($^{\cdot}OH$) and so on.[28,29] As well as non-radical species such as singlet oxygen ($^1O_2$)[30] are generated during activation of PMS.

However, the gradual increase in the types and concentrations of refractory organic pollutants in wastewater has placed higher demands on the treatment methods of wastewater, so many researchers have developed the synergy of different treatment technologies to treat refractory organic pollutants, such as electrochemical AOPs coupled with PMS, Fenton/PS, photocatalytic/PS, *etc.*[31–34] Through a review of different AOPs, it was found that the effect of iron sludge in Fenton can be solved by introducing electrochemistry to form an E-Fenton process, and it was found that there is a commonality between the E-Fenton process and the Fenton-like process for PMS activation (both require metal/metal ions for activation). Thus, the idea of E-Fenton oxidation processes coupled with PMS was proposed, in which ZVI and electricity act as a "bridge" between E-Fenton and PMS. So that this process can generate H_2O_2 while activating PMS efficiently, and Fenton reaction occurs through ZVI for activation, while the generated Fe(III) achieves Fe(III)/Fe(II) cycle at the cathode to strengthen the activation effect on the process, which not only has the advantages of the above research, but also solves most of the shortcomings of the above research.

E-Fenton can produce H_2O_2 at the cathode and can continuously give electrons in the cathodic reduction to promote the

circulation of Fe(III)/Fe(II) in solution and on the ZVI surface in the presence of an electric field. GF is widely used at the cathode due to its high surface area and low cost, but no study has been reported on GF as both the cathode and anode of the process in activated persulfate systems. In previous studies either electrochemically activated persulfates or electrochemically assisted iron-based activated persulfates have been used, but few studies have used GF as cathode and anode to treat pollutants by simultaneously acting all three processes: electro-activated PMS, ZVI-activated persulfate and electro-Fenton and fully considering the relative contribution of various ROS and reaction types.

In this study, we combined two AOPs based on different radicals, E-Fenton process and activated PMS process, to form the ZVI-E-Fenton-PMS process. The process mainly produced active substances by E-Fenton process, E-PMS process and ZVI-PMS process, and the simulated MB wastewater was used as the target pollutant to verify its effectiveness as well as its superiority. The main objectives of this study are to: (1) investigate the superiority of activated PMS process in combination with E-Fenton process for MB removal, (2) estimate the relative contribution of various reactions in the ZVI-E-Fenton-PMS process to MB removal and to determine the types of ROS in the process, and (3) explore the degradation mechanism and potential application of the ZVI-E-Fenton-PMS process.

2 Materials and methods

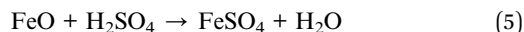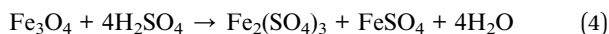### 2.1 Reagent and material

The drugs used in this study were all analytical grade reagents and were not further purified. The standards of methylene blue (MB), phenol, 1,10-phenanthroline 5,5-dimethyl-1-pyrroline N-oxide (DMPO) were obtained from Macklin Bio-Chem Technology Co., Ltd, China. Analytical grade potassium monopersulfate triple salt (PMS, $KHSO_5 \cdot 0.5KHSO_4 \cdot 0.5K_2SO_4$), 2,2,6,6-tetramethyl-4-piperidinyloxyl (TEMP), hydrogen peroxide (H_2O_2), ferrous sulfate heptahydrate ($FeSO_4 \cdot 7H_2O$), sodium sulphate (Na_2SO_4), anhydrous methanol (MeOH), *tert*-butanol (TBA), furfuryl alcohol (FFA) and sodium hydroxide (NaOH) were purchased from Aladdin Bio-Chem Technology Co., Ltd, China. Hydrochloric acid (HCl), acetone and sulfuric acid (H_2SO_4) were purchased from Tianjin Fengfan Chemical Reagent Technology Co., Ltd, China. GF was obtained from Suzhou Yilong Energy Technology Co., Ltd, China. All experimental water was deionized water.

2.2 Experimental procedures

Pre-treatment of zero-valent iron, the reduced iron powder was soaked with 0.1 M H_2SO_4 for 10 min (acid washing removes the dense oxide layer from the ZVI surface (eqn (3)–(5))), then washed with acetone, and finally washed with deionized water to neutral, then filtered and put in a desiccator to dry. Pre-treatment of graphite felt, the graphite felt was placed in an ultrasonic cleaner with deionized water for 15 min, then added 0.1 M H_2SO_4 for 15 min and left for 1 h, soaked in acetone solution and sonicated for 30 min, then washed repeatedly with

deionized water until the pH was neutral and soaked overnight, and eventually, rinse the GF repeatedly with deionized water and then stored in oven at 80 °C for 12 h, subsequent storage in a desiccator. The distance between the anode (GF, 40 mm × 20 mm × 2 mm) and the cathode (GF, 40 mm × 20 mm × 2 mm) was 2 cm.

$$Fe_2O_3 + 3H_2SO_4 \rightarrow Fe_2(SO_4)_3 + 3H_2O \tag{3}$$

$$Fe_3O_4 + 4H_2SO_4 \rightarrow Fe_2(SO_4)_3 + FeSO_4 + 4H_2O \tag{4}$$

$$FeO + H_2SO_4 \rightarrow FeSO_4 + H_2O \tag{5}$$

All experiments were performed with GF as cathode and anode in 50 mg L^{-1} MB aqueous solution, to which 0.05 M Na$_2$SO$_4$ was added to the cell as the supporting electrolyte with fixed amounts of PMS (2 mM) and ZVI (2 mM) for each degradation experiment. The experiments were performed under DC power supply (3 V, in addition to investigating the effect of voltage on the degradation of the process), experimental temperature of 25 ± 2 °C, stirring speed of 600 rpm, and air was added to the cathode at a rate of 0.3 L min^{-1}, where the pH was adjusted with 0.1 M NaOH and 0.1 M H$_2$SO$_4$. All samples were acquired from the reaction solution and filtered using 0.22 μm polyether sulfone membranes, and the oxidation reactions were quenched with 0.2 ml MeOH for a certain period, to allow for subsequent instrumental analysis. The radical quenching experiments are the same as the above experimental procedure, and the amount of quenching agent added will be detailed in the text. All experiments took three parallel samples.

2.3 Analytical methods

The concentration of MB and total iron (*o*-phenanthroline spectrophotometry) were measured with the help of ultraviolet-visible spectroscopy (UV-vis, TU-1901, China) (instrument parameters: the maximum absorption wavelength of MB is 664 nm). The mineralization rate was measured using a total organic carbon (TOC) analyzer (TOC-L, Shimadzu, Japan) (instrument parameters: the determination time was about 3 min for TC and 4 min for IC, the TOC value is TC-IC; combustion temperature: 950 °C). X-ray photoelectron spectroscopy (XPS, K-alpha, USA) was performed to measure ZVI before and after the reaction, XPS data is peaked by XPS peak41 software. To determine the degradation mechanisms and the respective contributions of the relevant reactions in the ZVI-E-Fenton-PMS process, electron paramagnetic resonance (EPR, JES-FA200, Japan) (instrument parameters: microwave power: 0.99800 Mw; modulation frequency: 100 kHz; modulation amplitude 1G; scan width: 5 × 1 mT; scan time: 2 min) and radical quenching assays were employed using 5,5-dimethyl-1-pyrroline-N-oxide (DMPO) and 2,2,6,6-tethamethyl-4-piperidinol (TEMP) as spin-trapping agent of EPR and MeOH, TBA and FFA as quenchers to identify the main ROS involved in MB degradation. Eqn (6) was used to calculate the degradation rate. Fitted MB degradation curve by first-order kinetic eqn (7):

$$\eta = \frac{c_t}{c_0} \times 100\% \tag{6}$$

$$\ln\left(\frac{c_t}{c_0}\right) = -kt \tag{7}$$

where C_0 is the concentration of MB (mg L^{-1}) at the adsorption–desorption equilibrium state, C_t is the real-time concentration of MB (mg L^{-1}), η is the degradation rate of MB, and k is the first-order rate constant (min^{-1}).

3 Results and discussion

3.1 Removal efficiency of MB in various processes

Fig. 1(a) compares the removal efficiency of MB by different processes. The removal efficiency of the simulated aqueous solution of MB treated by PMS alone was very low, only 26.64% within 60 min, which was due to the low redox potential of PMS and the fact that only a small amount of $^1O_2$ could be generated by self-decomposition, making it difficult to directly oxidize complex pollutants like MB. The removal efficiency of MB by electrolysis alone was 58.3%, the degradation of MB mainly through the direct electron transfer (DET) of the anode, the electrosorption of GF and ·OH generated by electrolysis of aqueous at the GF anode., but still could not effectively degrade MB. While the removal efficiency reached 79.91%, 78.75% and 83.33% after the degradation experiments of MB by ZVI-activated PMS (ZVI-PMS) process, electro-activated PMS (E-PMS) process and electro-Fenton (E-Fenton) process, respectively, the ROS produced by these three processes were the main contributors of MB degradation, indicating that the ROS played a crucial role in this process. Most significantly, the removal efficiency of the ZVI-E-Fenton-PMS process achieved 91.8% at 30 min, and almost completely removed within 60 min, which shows that the ZVI-E-Fenton-PMS process has a better ability to remove pollutants than other processes. As shown in Fig. 1(b), the squared pseudo-first-order kinetic regression coefficients for all MB removal processes were larger than 0.96, which means that they were all consistent with pseudo-first-order reaction kinetics for the initial 30 min, and the respective rate constants and regression coefficients are shown in Table 1. ZVI-E-Fenton-PMS process was significantly more effective than ZVI-PMS process, E-PMS process and E-Fenton process for MB removal. For example, the rate constant and MB removal efficiency of ZVI-E-Fenton-PMS process is much higher than other processes. According to these results, the ZVI-E-Fenton-PMS process may be more effective for MB removal since it has a synergistic effect with the ZVI-PMS process, E-PMS process and E-Fenton process.

The UV-vis spectra of MB in ZVI-E-Fenton-PMS process with time are shown in Fig. 1(c), which shows that the MB has two different characteristic peaks at 664 nm and 292 nm, representing the chromophore absorption peak and the aromatic ring structure absorption peak, respectively. When the reaction reached 40 min, the absorption peak at 664 nm vanished and observation of the MB solution revealed that it was indeed completely discolored. The absorption peak at 292 nm also completely disappeared, this result is different from that of Song *et al.*[35] and indicates that the ZVI-E-Fenton-PMS process is better than other process.
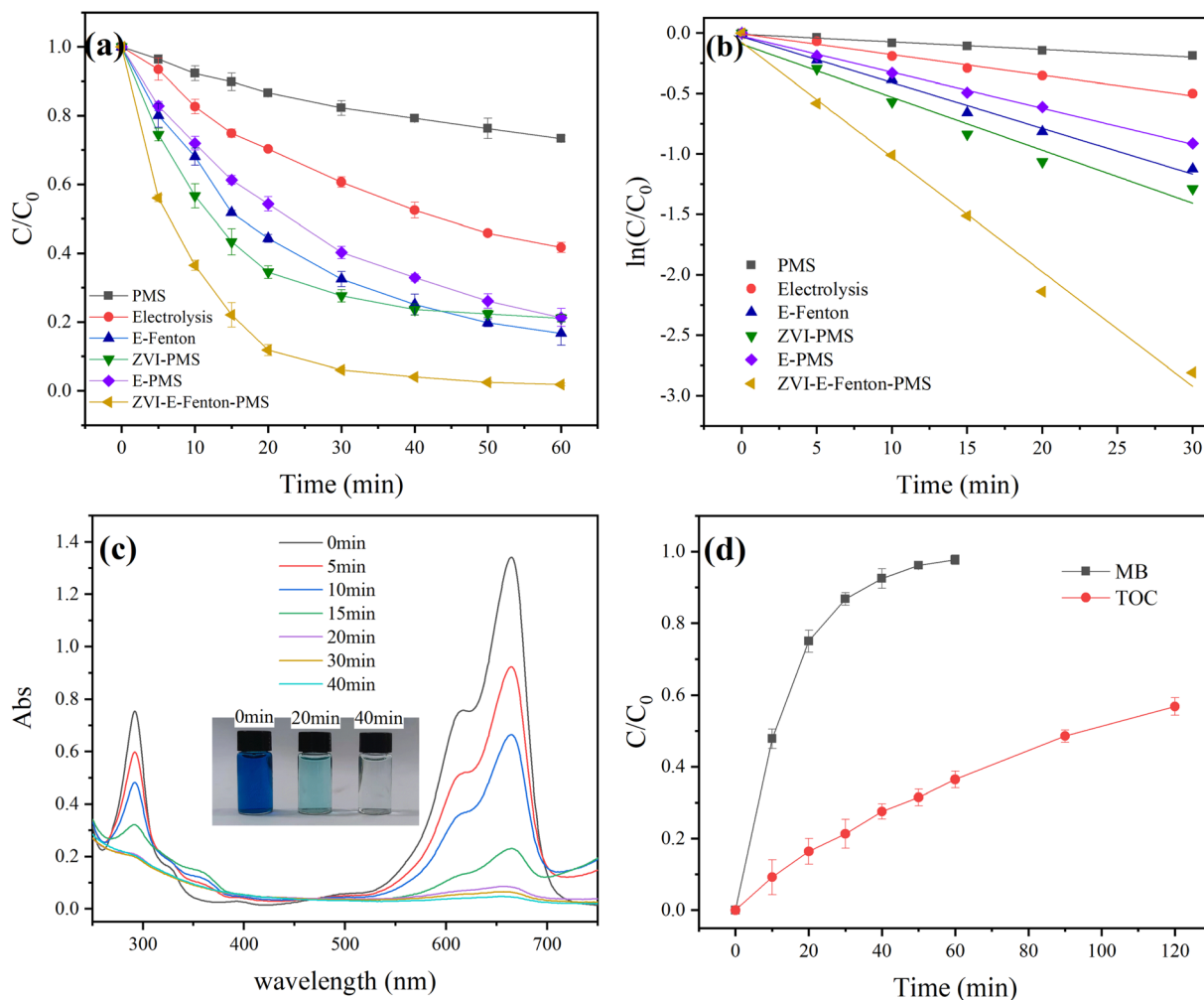
Fig. 1   (a) Removal efficiency of different systems; (b) influence of reaction kinetics; (c) UV-vis spectra of MB treated by ZVI-E-Fenton-PMS system at different times; (d) TOC removal rate (initial pH = 6; T = 25 ± 2 °C; stirring speed = 600 rpm; voltage = 3 V; [MB] = 50 mg L; [PMS] = 2 mM; [ZVI] = 2 mM; [Na$_2$SO$_4$] = 0.05 M).

To examine the mineralization effect of the ZVI-E-Fenton-PMS process during the treatment of MB wastewater, the total organic carbon (TOC) removal efficiency was used to describe the situation. The variation of TOC was recorded in Fig. 1(d). Within 60 min of the reaction, MB was completely removed, but the TOC removal efficiency was only 36.45%, and the TOC removal rate reached 56.83% when the duration of the experiment time was further expanded to 120 min. From the analysis of TOC and MB removal, we can know that the ZVI-E-Fenton-

PMS process can oxidize almost all MB to small molecule intermediates through the generated ROS, and the small molecules can be mineralized to H$_2$O, CO$_2$ and inorganic salts through further reactions (eqn (8) and (9)). Through the above analysis of the experimental data we can see that the ZVI-E-Fenton-PMS process is superior to other conventional processes, which reflects the superiority of this process.
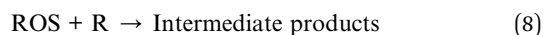
$$ROS + R \rightarrow \text{Intermediate products} \quad (8)$$

Table 1   Pseudo-first-order reaction kinetics constants for MB removal in different processes

Process name	Voltage (V)	PMS concentration (mmol L^{-1})	ZVI concentration (mmol L^{-1})	$k \times 10^{-2}$ (min^{-1})	R^2 (%)
PMS	Non	2.0	Non	0.63	98.37
Electrolysis	3.0	Non	Non	1.71	98.91
E-Fenton	3.0	Non	2.0	3.79	99.10
ZVI-PMS	Non	2.0	2.0	4.39	96.48
E-PMS	3.0	2.0	Non	2.98	99.74
ZVI-E-Fenton-PMS	3.0	2.0	2.0	9.49	99.10

$$\text{ROS + Intermediate products} \rightarrow H_2O + CO_2 \qquad (9)$$
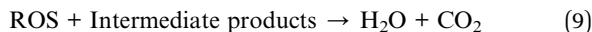
where R represents the pollutants, ROS mainly represent ˙OH, $SO_4^{\cdot-}$ and $^1O_2$ produced by ZVI-E-Fenton-PMS process.

The removal efficiency of the ZVI-E-Fenton-PMS system for MB was much higher than that of Liu et al.[36] using waste steel slag as a three-dimensional electrode for electrocatalytic degradation of 20 mg L^{-1} MB with a rate constant of 0.0266 min^{-1}, which was much smaller than the present system (0.0949 min^{-1}). As well as Han et al.[37] photo-catalytically combined with PMS, after modification, the combination with PMS was 4.6 times higher than that without combination, and the mineralization rate was greatly improved, and the miner-alization rate was 67% in 1 h, and the rate constant was 0.1328 min^{-1}, but the concentration of MB treated was only 2 × 10^{-5} M, and the concentration used in this process was about 10 times higher, so this process has good removal effect.

3.2 Effect of operating parameters

Investigating the impact of voltage on the ZVI-E-Fenton-PMS process is crucial since voltage affects the EAOPs significantly.

By raising the voltage from 2 V to 5 V, the influence of voltage on pollutant degradation was detected. As shown in Fig. 2(a), the MB removal efficiencies were 85.7%, 98.2%, 95.1% and 82.2% after 60 min of reaction when the voltages were 2 V, 3 V, 4 V and 5 V, respectively, and the reaction rate constants were 0.0424 min^{-1}, 0.0949 min^{-1}, 0.0721 min^{-1} and 0.0402 min^{-1}, respectively. The MB removal efficiency increased by 12.5% when the voltage increased from 2 V to 3 V. When the voltage further increased to 4 V the removal efficiency decreased slightly, and when it increased to 5 V it decreased directly to 82.2%. The possible reasons are: voltage has a certain influence on electron production, too low voltage will lead to the lack of direct anodic electron transfer, two-electron ORR reaction of cathode, and the ability to activate persulfate, in addition to the cycle of Fe^{3+}/Fe^{2+} in the process; the higher voltage generates more electrons and faster movement, thus accelerating the efficiency of direct anodic oxidation and cathodic activation of persulfate. However, too high voltage will cause a series of side reactions, including direct four-electron ORR, hydrogen evolu-tion reaction, H_2O_2 decomposition reaction, etc., which will affect its removal efficiency. Excessive voltage has a negative
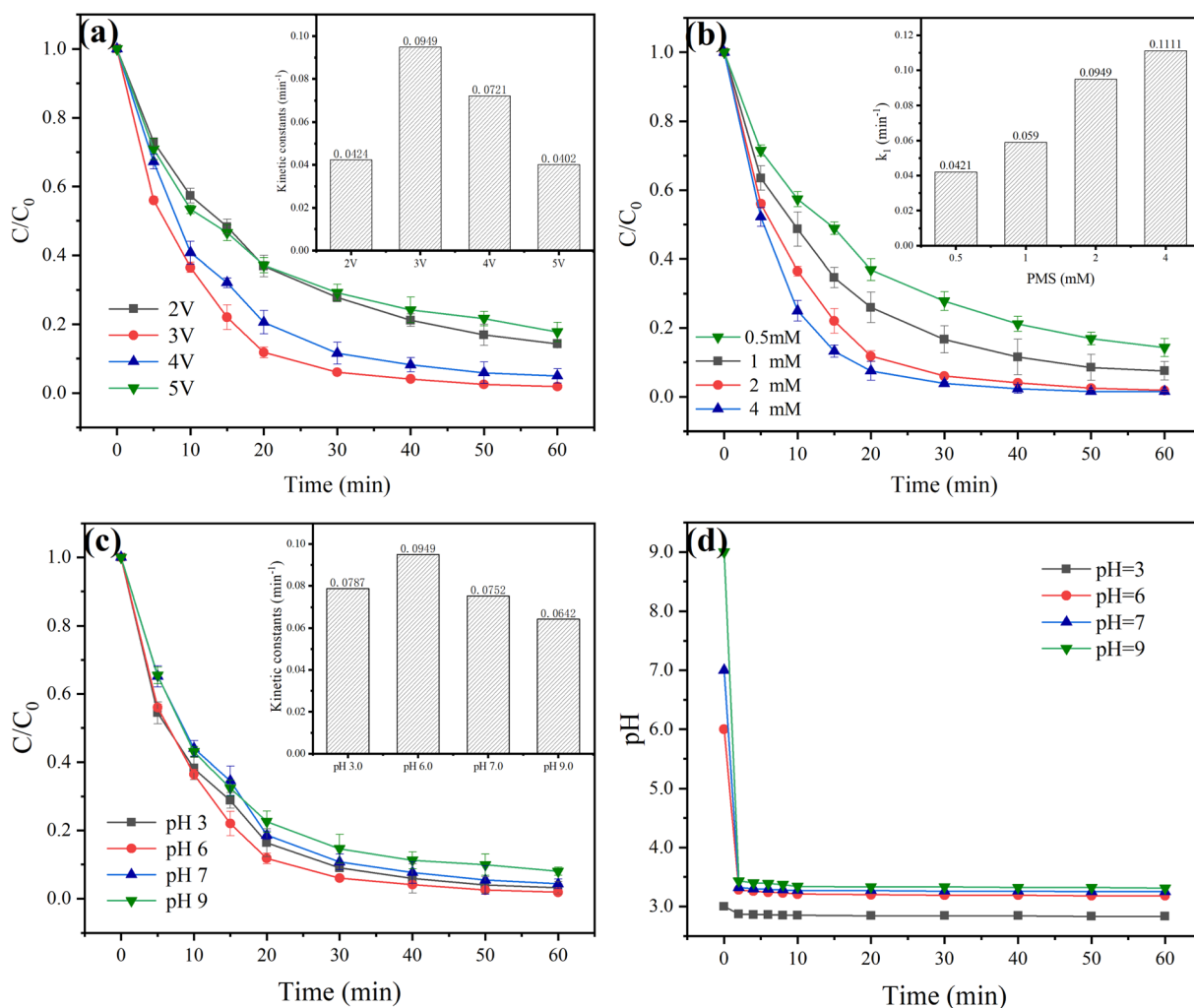

Fig. 2 Effect of operating conditions on the degradation of MB in the ZVI-E-Fenton-PMS process. (a) Voltage; (b) PMS concentration; (c) pH; (d) change of pH during the reaction ($T = 25 \pm 2$ °C; stirring speed = 600 rpm; voltage = 3 V; [MB] = 50 mg L; [ZVI] = 2 mM; [Na_2SO_4] = 0.05 M).

effect on the electrode itself and the removal efficiency, so the appropriate voltage is crucial for the process to degrade pollutants.

PMS is one of the most dominant oxidants in the ZVI-E-Fenton-PMS process. Experiments were conducted at PMS concentrations of 0.5 mM, 1 mM, 2 mM and 4 mM to evaluate the effect of PMS concentration on MB removal efficiency, as shown in Fig. 2(b). In the ZVI-E-Fenton-PMS process, PMS is the main source of $SO_4^{\cdot-}$, and more ROS are produced to degrade MB at higher PMS concentrations. When the PMS concentration increased from 0.5 mM to 2 mM, the MB removal efficiency increased from 85.7% to 98.2%, and the rate constant increased from 0.0421 min^{-1} to 0.0949 min^{-1}; further increasing the PMS concentration to 4 mM slightly increased the removal efficiency and rate constant to 98.5% and 0.1111 min^{-1}, respectively. The doubling of the PMS dosage resulted in only 0.3% increase in MB removal efficiency and a smaller increase in the reaction rate constant, which can be explained by the unfavorable depletion of $SO_4^{\cdot-}$ and $\cdot OH$ by the excess PMS, which allows the radicals to be scavenged or generate less reactive $SO_5^{\cdot-}$ and $\cdot HO_2$ with lower reactivity (eqn (10)), which affects their removal

efficiency. Thus, it was demonstrated that PMS is the most influential in the generation of ROS in the process.

Solution pH is a key parameter affecting ion distribution and ROS formation. Although acidity can provide a better redox potential, too much H^+ will consume $SO_4^{\cdot-}$ (eqn (11)), while being in alkaline conditions will form precipitates with the iron ions dissolved from ZVI, leading to the overwriting of the active site, and $SO_4^{\cdot-}$ will easily change to $\cdot OH$, and $\cdot OH$ also decreases the redox potential under alkaline conditions. Therefore, this part investigated the effect of initial pH on MB degradation, as shown in Fig. 2(c). pH changed from 3 to 6, and the MB degradation and removal efficiency increased further, while the MB removal efficiency decreased gradually from pH 6 to pH 9, but the degree of change was not significant, and all of them could reach more than 90%, indicating that the ZVI-E-Fenton-PMS process could achieve better MB removal in a wide range of initial pH. In order to investigate the change of pH after adding PMS to the solution, we monitored the pH of the solution during the experimental reaction, as shown in Fig. 2(d), when the initial pH was greater than 5, the pH dropped rapidly to within pH 4 after adding PMS at the initial stage,
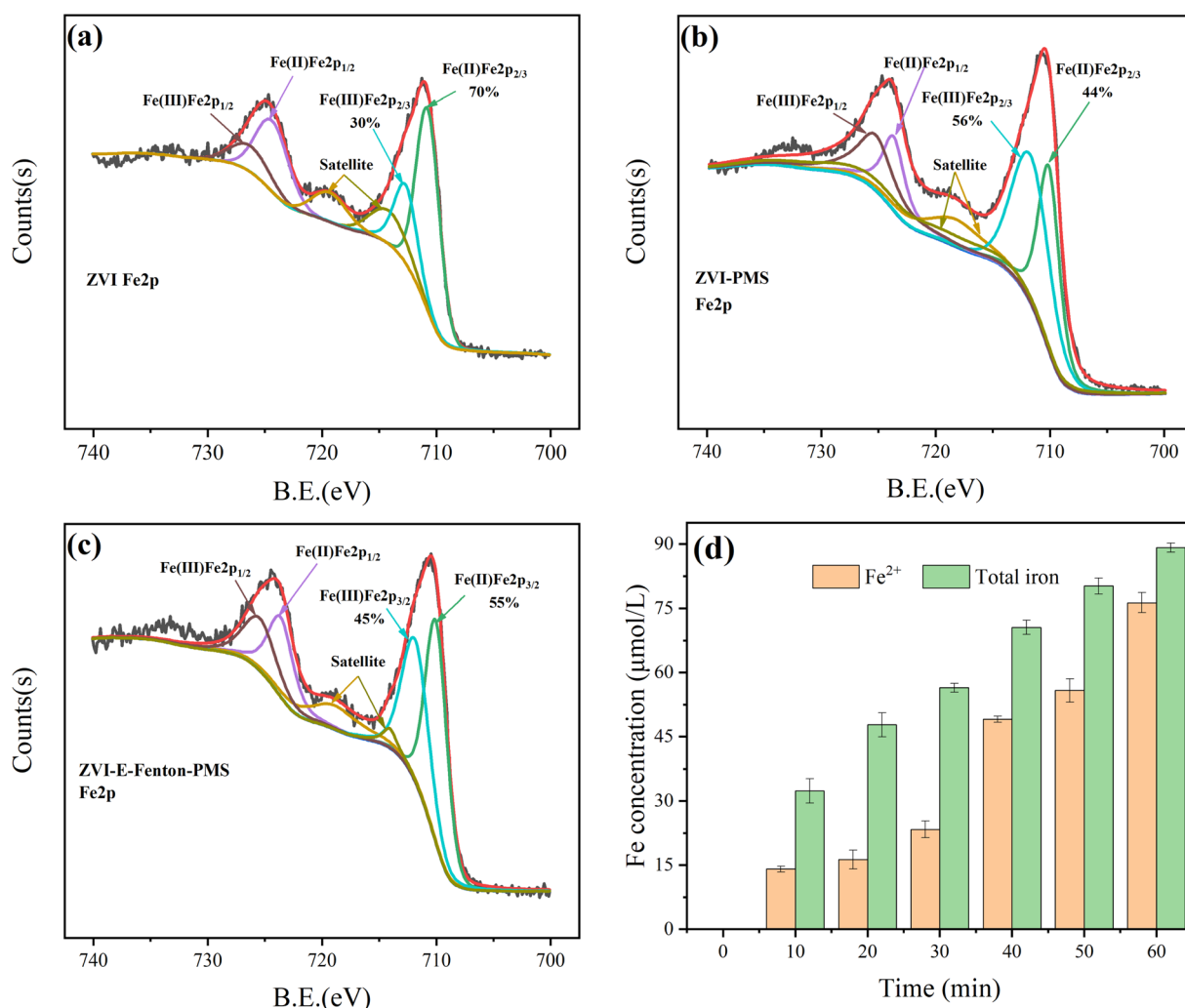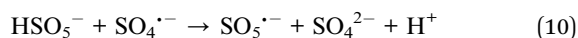

Fig. 3 Fe 2p XPS spectra for the ZVI (a) before; (b) after ZVI–PMS process; (c) after ZVI–E–Fenton–PMS process treatment; (d) valence change of iron ions in solution.

which was due to PMS could release large amounts of H$^+$ in water, thus it makes the solution acidic. The pH only dropped slightly at the later stage, which is due to the fact that the process of PMS activation generates H$^+$, which leads to a weak decrease in pH, and finally all of them can be stabilized within pH 4. This may be the reason why the initial pH change has less effect on MB degradation. It was observed that pH 3, pH 6 and pH 7 had similar final treatment efficiencies, but the k value was higher at pH 6 than the others, and the initial pH of the solution itself was at 6, which eliminated the need to adjust pH. Therefore, the best pH for MB degradation in this process was determined to be pH 6.

$$HSO_5^- + SO_4^{\bullet -} \rightarrow SO_5^{\bullet -} + SO_4^{2-} + H^+ \quad (10)$$

$$SO_4^{\bullet -} + H^+ + e^- \rightarrow HSO_4^{\bullet -} \quad (11)$$

3.3 The change in the ZVI surface before and after the reaction

The catalyst (ZVI) is an important component of the ZVI-E-Fenton-PMS process, and in order to investigate the reaction mechanism, XPS was used to analyze the change in the chemical valence of the ZVI surface. As shown in Fig. 3(a)–(c), the Fe2p 2/3 peaks at binding energies 710.1 eV and 712.1 eV are Fe(II) and Fe(III) on the surface of ZVI (before the reaction), such as FeO and Fe$_2$O$_3$ formed *in situ* on ZVI. Considering the evolution of two iron species in the ZVI-E-Fenton-PMS process, according to the respective peak areas, the relative proportion of Fe(II)/Fe(III) was detected on the surface of ZVI before the reaction is 2.33, and in the ZVI-PMS process, the relative ratio of Fe(II)/Fe(III) after the reaction is 0.79, with a wide range of decrease, which indicates that PMS and H$_2$O$_2$ are indeed activated by oxidation of divalent iron. Interestingly, the relative ratio of Fe(II)/Fe(III) of ZVI in the ZVI-E-Fenton-PMS process is 1.22, which is higher than the relative ratio of Fe(II)/Fe(III) of ZVI in the ZVI-PMS process. Theoretically the consumption of Fe(II) on the surface of ZVI should be higher than that of ZVI-PMS process, but the content of Fe(II) fraction on the surface of ZVI increases rather than decreases, which is due to the fact that Fe(III) on the surface of ZVI was continuously reduced to Fe(II) at the cathode. Therefore, the addition of EAOP not only promotes the activation of PMS by current, but also indirectly enhanced the activation of PMS by ZVI through the reduction of trivalent iron to divalent iron. The addition of EAOP can also increase the removal efficiency of pollutants through direct electron transfer and the formation of H$_2$O$_2$ at the cathode and Fenton reaction to produce $^\bullet$OH.

The iron concentration in the reaction solution was measured by *o*-phenanthroline spectrophotometry (as shown in Fig. 3(d)), it was found that the concentration of total iron has been increasing, which is caused by the continuous release of iron ions from ZVI, the concentration of Fe^{2+} is also increasing, and the proportion is getting larger and larger, reaching 85.6% at 60 min. The lowest proportion of Fe^{2+} was only 34.2% at 20 min, which was probably due to the fast reaction rate of

activated PMS and H$_2$O$_2$ consuming more Fe^{2+} at the early stage, and its consumption rate was higher than the rate of Fe^{2+} release from ZVI and Fe^{3+} reduction at the cathode, while the reduction of oxidant and pollutant concentration at the later stage resulted in not requiring too much ROS, and the rate of electrochemical reduction reached its peak, so the solution in the later stage of degradation is basically Fe^{2+}. And it was found that only 4.4% of the total iron was released into the reaction solution, it confirms that ZVI is consumed but less during the reaction and that these submerged iron species have little negative impact on MB degradation.

$$Fe(III) + e^- \rightarrow Fe(II) \quad (12)$$

$$Fe^{3+} + e^- \rightarrow Fe^{2+} \quad (13)$$
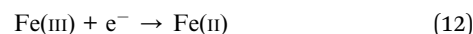
3.4 Mechanism study

3.4.1 Determination of the type of the ROS. ROS species in the ZVI-E-Fenton-PMS process are usually distinguished using quenching experiments, which take advantage of the different reaction rates of different scavengers with ROS. To explore the types of ROS in ZVI-E-Fenton-PMS process, the commonly used methyl alcohol (MeOH) and *tert*-butanol (TBA) as the scavenger for $^\bullet$OH and SO$_4^{\bullet -}$, and furfuryl alcohol (FFA) was served as the scavenger for ^{1}O$_2$. As shown in Table 2, TBA shows significantly higher reactivity with $^\bullet$OH than SO$_4^{\bullet -}$ (k_{TBA}, $^\bullet$OH = 6.0×10^8 M^{-1} s^{-1}, SO$_4^{\bullet -}$ = 7.6×10^5 M^{-1} s^{-1}), and the difference between $^\bullet$OH and SO$_4^{\bullet -}$ was three orders of magnitude. MeOH has high reactivity with $^\bullet$OH and SO$_4^{\bullet -}$ (k_{MeOH}, $^\bullet$OH = 9.7×10^8 M^{-1} s^{-1}, SO$_4^{\bullet -}$ = 2.5×10^7 M^{-1} s^{-1}). Therefore, in the process where $^\bullet$OH and SO$_4^{\bullet -}$ coexist, the types of radicals are often determined by adding MeOH and TBA to the system. In this experiment, 10 mM MeOH and TBA were added to the ZVI-E-Fenton-PMS process to verify the presence of $^\bullet$OH and SO$_4^{\bullet -}$. Since phenol is less polar than MeOH and TBA at room temperature, it can sufficiently quench radicals on the electrode and ZVI surfaces,[38] so it is possible to determine whether radicals are generated at the electrode and ZVI surfaces by adding 10 mM phenol.

As can be seen in Fig. 4(a), the removal efficiency of MB decreased from 93.96% to 87.03% after 30 min in the presence of TBA, which indicated that $^\bullet$OH plays an essential role in MB removal. Furthermore, in the presence of MeOH, MB removal efficiency decreased significantly from 93.96% to 69.21% after 30 min, which suggested that SO$_4^{\bullet -}$ also played an essential role

Table 2 Reaction rate constants between scavenger and ROS

	k $^\bullet$OH (M^{-1} s^{-1})	k SO$_4^{\bullet -}$ (M^{-1} s^{-1})	k ^{1}O$_2$ (M^{-1} s^{-1})
Phenol	8.8×10^9 (ref. 39)	6.6×10^9 (ref. 39)	Na
MeOH	9.7×10^8 (ref. 19)	2.5×10^7 (ref. 18)	3.0×10^3 (ref. 40)
TBA	6.0×10^8 (ref. 19)	7.6×10^5 (ref. 19)	1.8×10^3 (ref. 40)
FFA	1.5×10^{10} (ref. 19)	1.3×10^{10} (ref. 41)	1.2×10^8 (ref. 40)

for MB removal. Then, in the presence of phenol, the removal efficiency of MB decreased from 93.96% to 63.08% after 30 min in a higher range than that of MeOH, which showed that a part of the reaction does take place on the electrode and ZVI surface.

Many studies have demonstrated that $^1O_2$ can be produced in activated PMS processes. To determine whether $^1O_2$ is produced in this process, FFA was used as the scavenger for $^1O_2$, as shown in Table 2, its reaction rate constant with $^1O_2$ was 1.2 $\times 10^8$ M^{-1} s^{-1}, which was much higher than other scavengers, but its reaction rate constant with $^\cdot$OH and SO$_4^{\cdot-}$ were also as high as 1.5×10^{10} M^{-1} s^{-1} and 1.3×10^{10} M^{-1} s^{-1}, so the concentration of different scavengers was adjusted by adding different scavengers to ensure that the reaction rates of different scavengers with $^\cdot$OH and SO$_4^{\cdot-}$ were the same to determine the presence or absence of $^1O_2$. Therefore 6 mM FFA, 100 mM MeOH and 100 mM TBA were added respectively to ensure that the reaction rates with $^\cdot$OH and SO$_4^{\cdot-}$ were at the same order of magnitude, while the reaction rates of FFA with $^1O_2$ were three orders of magnitude higher than those of MeOH and TBA with

$^1O_2$. As shown in Fig. 4(b), the inhibition of MB degradation by the addition of FFA was significantly higher than that of MeOH and TBA, indicating that $^1O_2$ is present in the process and played a role.

To further verify the existence of $^\cdot$OH, SO$_4^{\cdot-}$ and $^1O_2$ in the process, electron paramagnetic resonance (EPR) technique was used to detect it. DMPO as the spin-trapping agent to capture $^\cdot$OH and SO$_4^{\cdot-}$ in the E-Fenton process, ZVI-PMS process, E-PMS process and ZVI-E-Fenton-PMS process. The characteristic peak signals of DMPO–SO$_4^{\cdot-}$ (characteristic intensity ratio 1 : 1 : 1 : 1 : 1 : 1) and DMPO-HO$^\cdot$ (characteristic intensity ratio of 1 : 2 : 2 : 1) adducts were evident in the ZVI-PMS process, E-PMS process and ZVI-E-Fenton-PMS process (Fig. 4(c)), and the characteristic peak signals of the two adducts in the ZVI-E-Fenton-PMS process were significantly higher than those in the ZVI-PMS process and E-PMS process. As expected, only the characteristic peak signal of DMPO-HO$^\cdot$ adduct was detected in the E-Fenton process, and the intensity of the characteristic peak signal was also significantly weaker than that of the ZVI-E-
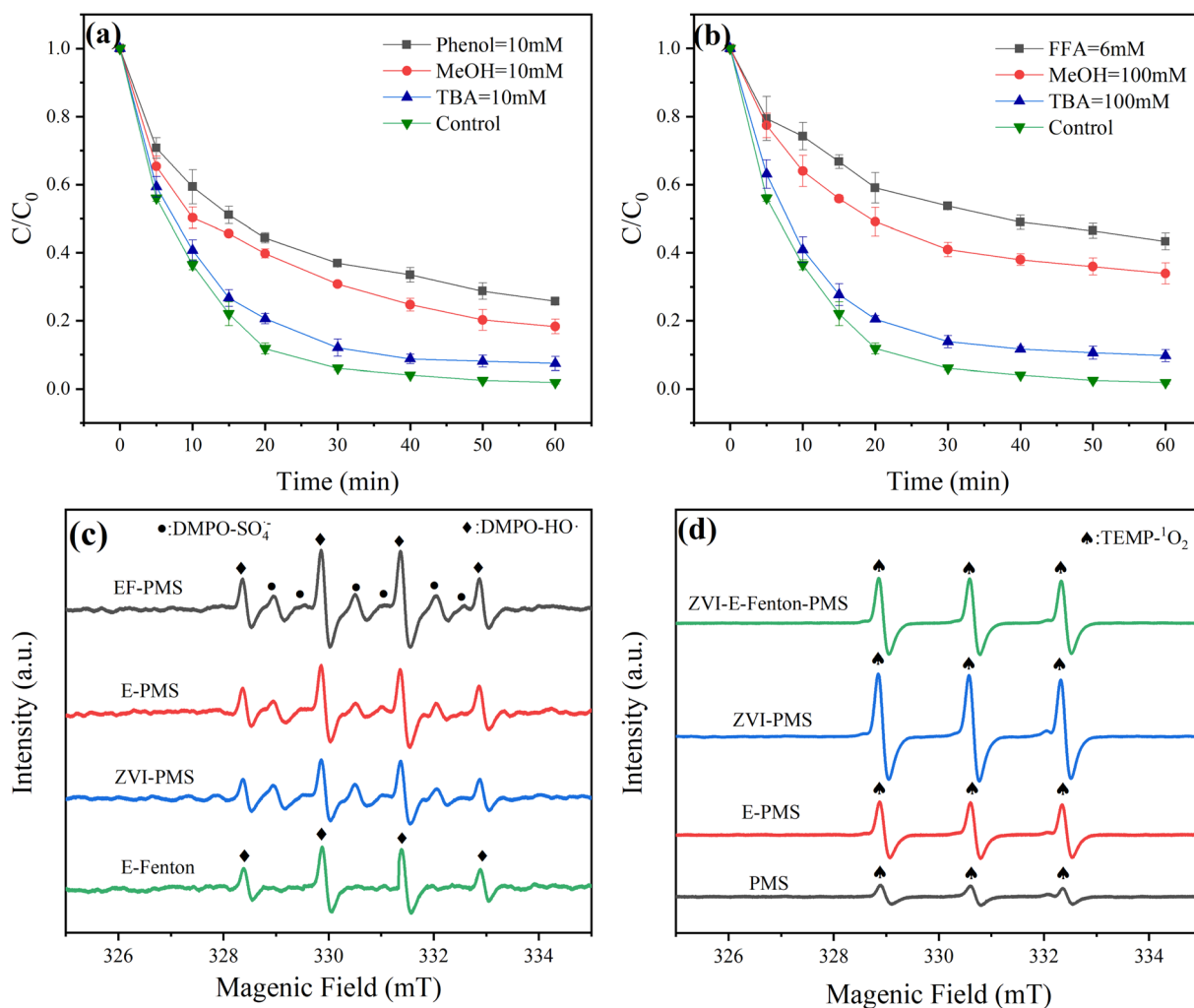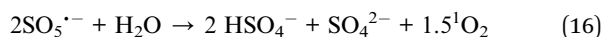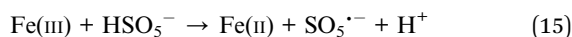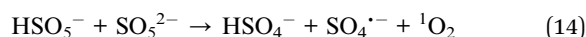

Fig. 4 (a) Effects of Phenol, MeOH and TBA (b) FFA, MeOH and TBA on MB removal by ZVI-E-Fenton-PMS process; EPR spectra for (c) $^\cdot$OH and SO$_4^{\cdot-}$, (d) $^1O_2$ (initial pH = 6; $T = 25 \pm 2$ °C; stirring speed = 600 rpm; voltage = 3 V; [MB] = 50 mg L; [PMS] = 2 mM; [ZVI] = 2 mM; [Na$_2$SO$_4$] = 0.05 M).

Fenton-PMS process. Therefore, it shows that the combination of E-Fenton and ZVI-PMS has a synergistic effect, which can favor the production of $^{\bullet}OH$ and $SO_4^{\bullet-}$. In addition, TEMP as the spin-trapping agent to capture the nonradical ROS $^1O_2$. As depicted in Fig. 4(d), a small triple EPR characteristic peak signal was detected after mixing TEMP with PMS, which was observed mainly due to the reaction of TEMP with $^1O_2$ generated by the self-decomposition of PMS (eqn (14)) to form the TEMP-$^1O_2$ (characteristic intensity ratio of $1:1:1$) adduct.[42] Interestingly, the signal intensity of the characteristic peaks of the TEMP-$^1O_2$ adducts of PMS process, E-PMS process and ZVI-PMS process gradually increased, while the intensity of the characteristic peak signal of the ZVI-E-Fenton-PMS process was weaker than that of the ZVI-PMS process, and in contrast to Fig. 4(c), the signal intensities of characteristic peaks of DMPO–$SO_4^{\bullet-}$ and DMPO-HO$^{\bullet}$ of the ZVI-PMS process were significantly weaker than those of ZVI-E-Fenton-PMS process, which is probably due to the fact that the ZVI-E-Fenton-PMS process has more electrochemical assistance compared to the ZVI-PMS process making the solution and ZVI surface less divalent iron, thus reducing the trivalent iron consumption of PMS to generate $SO_5^{\bullet-}$, which further generates $^1O_2$ (eqn (15) and (16)), allowing more PMS to be used to generate $^{\bullet}OH$ and $SO_4^{\bullet-}$, which also precisely reflects the synergistic effect of the process. In summary, the radical quenching experiments and EPR tests demonstrated that the main ROS for MB degradation in the ZVI-E-Fenton-PMS process were $^{\bullet}OH$, $SO_4^{\bullet-}$ and $^1O_2$.

$$HSO_5^- + SO_5^{2-} \rightarrow HSO_4^- + SO_4^{\bullet-} + {}^1O_2 \quad (14)$$

$$Fe(III) + HSO_5^- \rightarrow Fe(II) + SO_5^{\bullet-} + H^+ \quad (15)$$

$$2SO_5^{\bullet-} + H_2O \rightarrow 2HSO_4^- + SO_4^{2-} + 1.5{}^1O_2 \quad (16)$$

3.4.2 Estimation of the contribution of involved reactions.
MB degradation in the ZVI-E-Fenton-PMS process is mainly *via* the following pathways: (1) direct electron transfer (DET) in combination with GF electrosorption; (2) direct oxidation by PMS; (3) oxidation by ROS ($^{\bullet}OH$, $SO_4^{\bullet-}$ and $^1O_2$) and (4) non-ROS

oxidation. In order to clarify the contribution of various degradation pathways, a two-step combination of complete capture-competitive reaction kinetics was used to obtain the reaction rate constants of the above pathways by experimental design. In this experiment, it was assumed that the addition of 10 M MeOH to the ZVI-E-Fenton-PMS process could scavenge all available $^{\bullet}OH$, $SO_4^{\bullet-}$ and $^1O_2$ completely and 0.7 M TBA could scavenge $^{\bullet}OH$ completely. The estimation process and results of the contribution of each relevant reaction in the ZVI-E-Fenton-PMS process are shown in Table 3.

As shown in Table 3, the contribution of DET in combination with GF electroadsorption, direct oxidation by PMS and non-ROS oxidation to the ZVI-E-Fenton-PMS process were only 6.74%, 3.37% and 5.16%, respectively, and the total contribution of the three modalities was less than 16%, while the contribution of ROS reached 85.77%, in which the contribution of ROS generated by direct electrolysis (D_1) to MB degradation was only 11.27%, while the contribution of ROS generated by E-Fenton process, E-PMS process and ZVI-PMS process (D_2) was 74.50%, indicating that it was the primary way to remove pollutants in ZVI-E-Fenton-PMS process. The relative contribution of each ROS to MB removal was estimated using competitive kinetic experiments, and the calculated results are summarized in Table 4, according to eqn (17)–(19). The relative contributions of $^{\bullet}OH$, $SO_4^{\bullet-}$ and $^1O_2$ in the process were 30.77%, 39.62% and 15.38%, respectively.

$$R_{{}^1O_2} = \frac{k_{obs1} - k_{obs2}}{k_{obs}} \quad (17)$$

$$R_{SO_4^{\bullet-}} = \frac{k_{SO_4^{\bullet-}}}{k_{obs}} = \frac{k_{TBA} - k_{obs2} - k_{{}^1O_2}}{k_{obs}} \quad (18)$$

$$R_{\bullet OH} = \frac{k_{\bullet OH}}{k_{obs}} = \frac{k_{ROS} - k_{SO_4^{\bullet-}} - k_{{}^1O_2}}{k_{obs}} \quad (19)$$

where R$^{\bullet}$OH, R$SO_4^{\bullet-}$ and R$^1O_2$ are referred to as the relative contributions of $^{\bullet}OH$, $SO_4^{\bullet-}$ and $^1O_2$, kobs1, kobs2, kobs and kROS represent the apparent pseudo-first-order kinetic rate constants for MB removal by the ZVI-E-Fenton-PMS process at

Table 3 The relative contribution of the various reaction types in ZVI-E-Fenton-PMS process (initial pH = 6; $T = 25 \pm 2$ °C; stirring speed = 600 rpm; voltage = 3 V; [MB] = 50 mg L; [PMS] = 2 mM; [ZVI] = 2 mM; [Na$_2$SO$_4$] = 0.05 M)[a,b,c,d]

Process	Reaction types	Apparent degradation rate constant of MB ($\times 10^{-2}$ min^{-1})	Contribution (%)
ZVI-E-Fenton-PMS	A + B + C + D	9.49	100.00
Electrolysis alone-10 M MeOH	A	0.64	6.74
Electrolysis alone	A + D$_1$	1.71	
PMS alone-10 mM FFA	B	0.32	3.37
ZVI-E-Fenton-PMS-10 M MeOH	A + B + C	1.45	
ZVI-E-Fenton-PMS-0.7 M TBA		6.67	
	C	0.49	5.16
	D$_1$	1.07	11.27
	D$_2$	7.07	74.50
	D	8.14	85.77

[a] A: Direct electron transfer in combination with GF electrosorption. [b] B: PMS alone oxidation. [c] C: Non-ROS reaction. [d] D: ROS oxidation (D = D$_1$ + D$_2$).

RSC Advances

Paper

Table 4 Contribution rate of ROS in MB removal by ZVI-E-Fenton-PMS process (initial pH = 6; T = 25 ± 2 °C; stirring speed = 600 rpm; voltage = 3 V; [MB] = 50 mg L; [PMS] = 2 mM; [ZVI] = 2 mM; [Na$_2$SO$_4$] = 0.05 M)

	k ROS	k $^{\cdot}$OH	k SO$_4^{\cdot-}$	k ^{1}O$_2$
Rate constant (min^{-1})	0.0814	0.0292	0.0376	0.0146
Contribution to ROS (%)	100.00	35.87	46.19	17.94
Contribution to ZVI-E-Fenton-PMS process (%)	85.77	30.77	39.62	15.38

100 mM methanol, the combined action of A, B, C, the MB removal by the ZVI-E-Fenton-PMS process, and the MB removal by all ROS in the ZVI-E-Fenton-PMS process, respectively. All data are shown in Table 3.

3.4.3 Effect of different PMS doses on the contribution of various reactions. In order to investigate the relative contribution ratio of the ROS that optimally treat pollutants in the ZVI-E-Fenton-PMS process, we used the same method as in Section 3.4.2 to estimate the relative contribution of the ROS to MB degradation by varying the PMS dose, the condition that mainly affects the production of ROS in the ZVI-E-Fenton-PMS process. Table 5, Tables 3 and 6 show the estimated contributions of the various reactions involved in the ZVI-E-Fenton-PMS process at PMS doses of 1 mM, 2 mM and 4 mM, respectively.

Through Fig. 5(b), we can see that the relative contributions of SO$_4^{\cdot-}$, $^{\cdot}$OH and ^{1}O$_2$ in the ZVI-E-Fenton-PMS process were 37.80%, 12.71% and 28.98%, respectively, at a PMS dose of

1 mM; at a PMS dose of 2 mM, the relative contributions of SO$_4^{\cdot-}$, $^{\cdot}$OH and ^{1}O$_2$ in the ZVI-E-Fenton-PMS process were 39.62%, 30.77% and 15.38%, respectively; at the PMS dose of 4 mM, the relative contributions of SO$_4^{\cdot-}$, $^{\cdot}$OH and ^{1}O$_2$ in the ZVI-E-Fenton-PMS process were 24.39%, 38.52% and 3.24%, respectively. As shown in Fig. 5(a), with the increase of PMS dose, the removal efficiency of MB by ZVI-E-Fenton-PMS process increased accordingly, and the proportion of the relative contribution of ROS in the ZVI-E-Fenton-PMS process is increasing for free radicals, especially $^{\cdot}$OH, and decreasing for ^{1}O$_2$, and the proportion of non-ROS oxidation was more and more, indicating that non-ROS oxidation also plays an important role. The relative contribution of non-ROS oxidation is greatly enhanced at the PMS dose of 4 mM compared with other doses, which may be due to the relative excess of PMS, which is excited into a transition state molecular structure (eqn (20) and (21)) at the anode under the effect of electrochemistry, and its

Table 5 The relative contribution of the various reaction types in ZVI-E-Fenton-PMS process (initial pH = 6; T = 25 ± 2 °C; stirring speed = 600 rpm; voltage = 3 V; [MB] = 50 mg L; [PMS] = 1 mM; [ZVI] = 2 mM; [Na$_2$SO$_4$] = 0.05 M)

Process	Reaction types	Apparent degradation rate constant of MB (×10^{-2} min^{-1})	Contribution (%)
ZVI-E-Fenton-PMS	A + B + C + D	5.90	100.00
Electrolysis alone-10 M MeOH	A	0.64	6.74
Electrolysis alone	A + D$_1$	1.71	
PMS alone-10 mM FFA	B	0.11	1.86
ZVI-E-Fenton-PMS-10 M MeOH	A + B + C	1.21	
ZVI-E-Fenton-PMS-0.7 M TBA		5.15	
	C	0.46	7.80
	D$_1$	1.07	11.27
	D$_2$	3.62	61.36
	D	4.69	79.49

Table 6 The relative contribution of the various reaction types in ZVI-E-Fenton-PMS process (initial pH = 6; T = 25 ± 2 °C; stirring speed = 600 rpm; voltage = 3 V; [MB] = 50 mg L; [PMS] = 4 mM; [ZVI] = 2 mM; [Na$_2$SO$_4$] = 0.05 M)

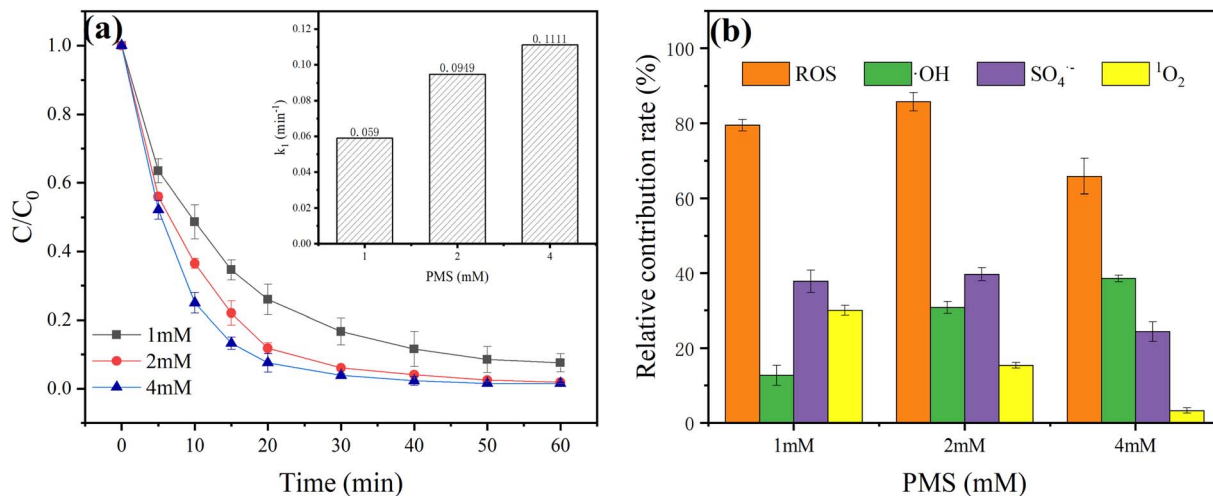| Process	Reaction types	Apparent degradation rate constant of MB (×10^{-2} min^{-1})	Contribution (%)
ZVI-E-Fenton-PMS	A + B + C + D	11.11	100.00
Electrolysis alone-10 M MeOH	A	0.64	6.74
Electrolysis alone	A + D$_1$	1.71	
PMS alone-10 mM FFA	B	0.68	6.12
ZVI-E-Fenton-PMS-10 M MeOH	A + B + C	3.76	
ZVI-E-Fenton-PMS-0.7 M TBA		6.83	
	C	2.44	21.96
	D$_1$	1.07	11.27
	D$_2$	6.28	56.53
	D	7.35	66.16

Fig. 5 Different PMS doses (a) degradation efficiency and its (b) relative contribution of different ROS by ZVI-E-Fenton-PMS process (initial pH = 6; $T = 25 \pm 2$ °C; stirring speed = 600 rpm; voltage = 3 V; [MB] = 50 mg L; [ZVI] = 2 mM; [Na$_2$SO$_4$] = 0.05 M).

oxidation capacity is greater than that of PMS, thus promoting the degradation of pollutants.[43]

$$C–HSO_5^- \rightarrow C*HSO_5^- \tag{20}$$

$$C*HSO_5^- + R \rightarrow \text{Intermediate products} + SO_5^{2-} + H^+ \tag{21}$$
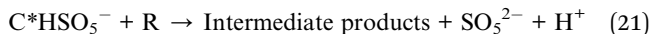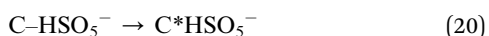
Where C represents the GF electrode surface and R represents the pollutants.

3.4.4 Proposed mechanism. Through the above analysis, the reasonable mechanism of the ZVI-E-Fenton-PMS process to treat pollutants is shown in Fig. 6. Few pollutants are removed by DET, GF electrosorption and PMS direct oxidation, the oxidation of ROS plays a dominant role. The generation of ROS mainly includes two pathways: E-Fenton and PMS activation, while the activation of PMS can be divided into two pathways: electric activation and ZVI activation.
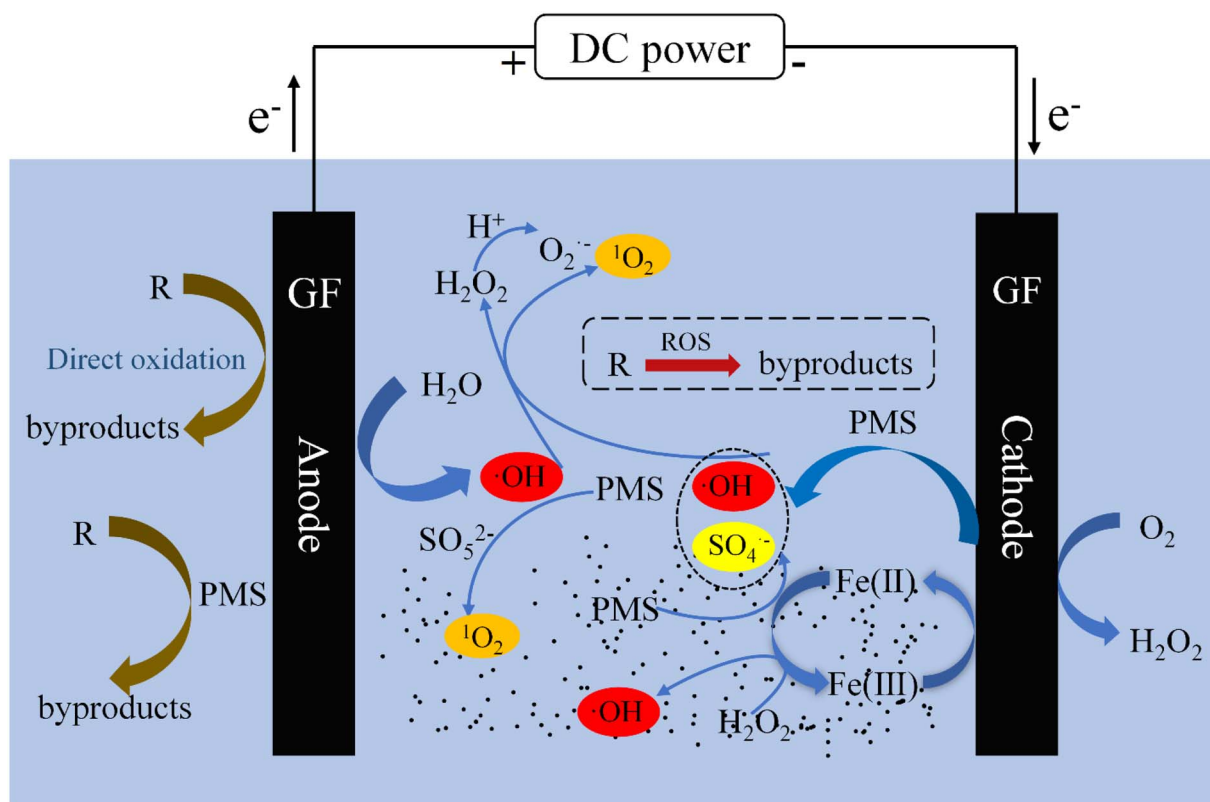

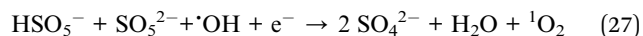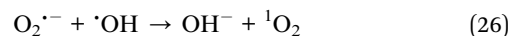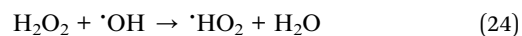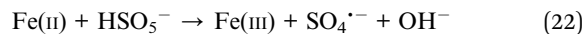Fig. 6 Possible oxidation mechanism of ZVI-E-Fenton-PMS process.

The principle of the E-Fenton part is very simple. Firstly, the cathode in the ZVI-E-Fenton-PMS process will undergo an ORR reaction to produce H_2O_2 *in situ*, and then a Fenton reaction with the ferrous ions in the process to produce $^\bullet OH$ (eqn (1) and (2)). In the PMS activation part, on the one hand, PMS undergoes a Fenton-like reaction with Fe(II) on the surface of ZVI or with Fe^{2+} in solution to produce $SO_4^{\bullet-}$ (eqn (22)), $SO_5^{\bullet-}$ will also be generated along with the reaction of Fe(III) with HSO_5^- (eqn (15)), while Fe(III) will also be reduced to Fe(II) at the cathode or by reaction with ZVI (eqn (12) and (13)), further promoting PMS activation. On the other hand, electro-activation of PMS also produces $SO_4^{\bullet-}$ and $^\bullet OH$, the main mechanism is that HSO_5^- gains electrons at the cathode to produce $SO_4^{\bullet-}$ and $^\bullet OH$ (eqn (3)), and there is also a conversion of $SO_4^{\bullet-}$ to $^\bullet OH$ in the process (eqn (23)).

In addition, the activation of PMS in the ZVI-E-Fenton-PMS process to produce $SO_4^{\bullet-}$ and $^\bullet OH$ is accompanied by the generation of the nonradical $^1O_2$, a highly selective oxidant that reacts almost exclusively with unsaturated organic matter through electrophilic addition and electron transfer.[44] Its generation mainly includes: (1) PMS self-decomposition to produce $^1O_2$ (eqn (14)), as shown in Fig. 4(d), where PMS alone formed a TEMP-$^1O_2$ adduct with TEMP without the addition of any catalyst; (2) the H_2O_2 produced in the process reacts with $^\bullet OH$ to produce $^1O_2$ (eqn (24)–(26));[45,46] (3) the generated $^\bullet OH$ likes to adsorb on the ZVI surface, and then ZVI triggers a surface-bound $^\bullet OH$-mediated reaction to produce $^1O_2$,[47] this reveals why the characteristic peak signal of the TEMP-$^1O_2$ adduct of the ZVI-PMS process is higher than that of the other processes in Fig. 4(d); (4) $^\bullet OH$ promotes the formation of $^1O_2$ in the presence of an electric field (eqn (27)).[48] The analysis of 3.4.3 section reveals that the relative contribution of $^1O_2$ is high when the relative contribution of $^\bullet OH$ is low, which suggesting that (4) may be the main way to produce $^1O_2$.

In the electrochemical process, PMS is excited to $C^*HSO_5^-$ on the anode surface, which has higher reactivity and can directly oxidize the MB adsorbed on the GF anode. In summary, the degradation of MB by the ZVI-E-Fenton-PMS process is accomplished by the combination of ROS oxidation, DET and GF electrosorption, direct oxidation by PMS and non-ROS oxidation. Overall oxidation mechanisms were summarized in Fig. 6.

In summary, we can learn that the degradation of MB in this study mainly comes from the oxidation of ROS, in which single $^\bullet OH$ can degrade MB into small molecules through substitution, addition and electron transfer reactions, but $^\bullet OH$ is not selective and has a short half-life, which makes it weak in opening the aromatic ring structure of MB (as discussed in Section 3.1) and requires a large number of $^\bullet OH$. In contrast, ZVI-E-Fenton-PMS process can produce a variety of ROS, among which the redox potential and half-life of $SO_4^{\bullet-}$ are larger than $^\bullet OH$, theoretically better removal. In this process multiple ROS can complement each other in the process of treating pollutants in synergy. The ROS with strong oxidizing ability can open the ring of aromatic ring into small molecules, and the ROS with weak oxidizing ability can oxidize the small molecules, in this process, each ROS can perform its own function to degrade the

pollutants and finally mineralize them into H_2O, CO_2 and inorganic salts.

$$Fe(II) + HSO_5^- \rightarrow Fe(III) + SO_4^{\bullet-} + OH^- \tag{22}$$

$$SO_4^{\bullet-} + H_2O \rightarrow {}^\bullet OH + H^+ + SO_4^{2-} \tag{23}$$

$$H_2O_2 + {}^\bullet OH \rightarrow {}^\bullet HO_2 + H_2O \tag{24}$$

$$^\bullet HO_2 \rightarrow H^+ + O_2^{\bullet-} \tag{25}$$

$$O_2^{\bullet-} + {}^\bullet OH \rightarrow OH^- + {}^1O_2 \tag{26}$$

$$HSO_5^- + SO_5^{2-} + {}^\bullet OH + e^- \rightarrow 2\, SO_4^{2-} + H_2O + {}^1O_2 \tag{27}$$

3.4.5 Removal efficiency of different organic pollutants. To further demonstrate the universality of the ZVI-E-Fenton-PMS process in wastewater treatment, we investigated its suitability for the degradation of four different organic pollutants, namely, methylene blue (MB), methyl orange (MO), berberine hydrochloride (BBH) and *p*-nitrophenol (PNP). It can be seen from the Fig. 7 that the removal efficiency of MB, MO and PNP can reach more than 94% within 60 min, while BBH required a longer time to be eliminated, 89.52% of BBH was removed within 60 min. In summary, it can be shown that the ZVI-E-Fenton-PMS process is a good system to remove refractory organic pollutants.

3.4.6 Stability of catalyst and process. The good catalytic effect of ZVI and the stability of ZVI-E-Fenton-PMS process achieve a good MB degradation efficiency. To evaluate the reusability of ZVI and ZVI-E-Fenton-PMS process, we then conducted ZVI reuse experiments and continuous degradation experiments of pollutants, respectively. As shown in Fig. 8(a), we found that the MB removal efficiency decreased by only 3.6% after five cycles, indicating that ZVI could be recycled and
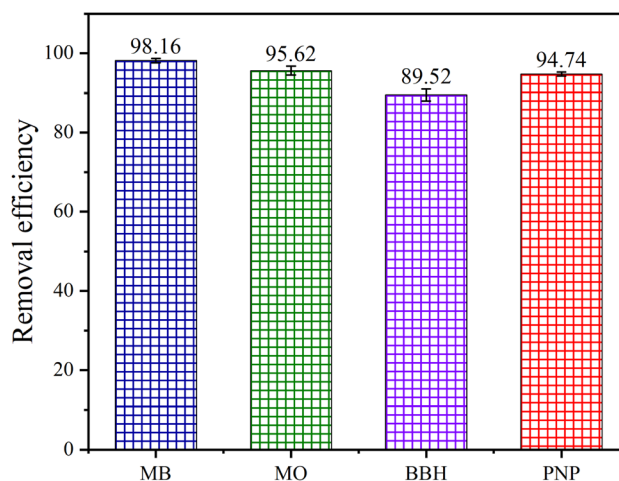
Fig. 7 Removal efficiency of different organic pollutants in ZVI-E-Fenton-PMS process (initial pH = 6; $T = 25 \pm 2$ °C; stirring speed = 600 rpm; voltage = 3 V; [MB] = [MO] = [BBH] = [PNP] = 50 mg L; [PMS] = 2 mM; [ZVI] = 2 mM; [Na$_2$SO$_4$] = 0.05 M).
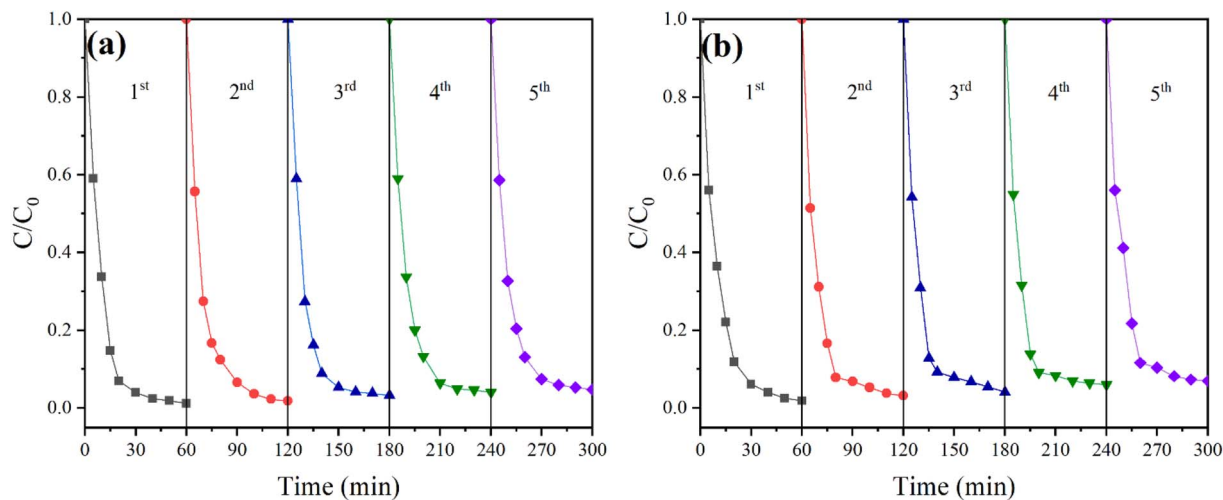
Fig. 8 Stability of (a) ZVI and (b) ZVI-E-Fenton-PMS processes (initial pH = 6; $T = 25 \pm 2$ °C; stirring speed = 600 rpm; voltage = 3 V; [MB] = 50 mg L; [PMS] = 2 mM; [ZVI] = 2 mM; [Na$_2$SO$_4$] = 0.05 M).

maintained its good catalytic performance after use. As shown in Fig. 8(b), after five consecutive pollutant degradation tests in ZVI-E-Fenton-PMS process, the removal efficiency of MB can still reach 93%, only reducing by 6%, which demonstrates that the process has good stability. The decrease in degradation efficiency in continuous degradation experiments may be mainly attributed to GF anodic oxidation and ZVI covering the active sites indicated by GF electrodes, resulting in a decrease in GF electrode performance.[43]

4 Conclusions

In this study, the combination of peroxymonosulfate (PMS) and E-Fenton with ZVI as the catalyst (ZVI-E-Fenton-PMS) was systematically investigated and the process was found to exhibit high MB removal efficiency and demonstrated the synergistic interaction between different AOPs as well as ROS. By comparing ZVI-E-Fenton-PMS process with other processes, we found that its removal efficiency and reaction rate constant are much higher than other processes, its MB removal rate and reaction rate constant are 98.16% and 0.0949 min^{-1}. The species of ROS in the process were determined by quenching experiments and EPR, mainly including $^{\bullet}$OH, SO$_4^{\bullet-}$ and ^{1}O$_2$, and the relative contributions of the involved reactions were determined by competitive kinetic experiments, and ROS were discovered to play a dominant role in MB degradation, with a relative contribution of 85.77%. XPS and o-phenanthroline spectrophotometry confirm the sustainable Fe(III)/Fe(II) redox cycle at the cathode, indicating that the addition of EAOP improved the catalytic and utilization efficiency of ZVI. The experimental operating conditions were 2 mM of ZVI dosage, 2 mM of PMS dosage, pH = 6, and 3 V of voltage, showing lower energy requirements. This process takes advantage of the different properties of different ROS and non-ROS to form a complementary advantage, further elaborating the synergy between ROS oxidation and non-ROS oxidation of the ZVI-E-Fenton-PMS process. Finally, the process is subjected to five consecutive contaminant degradation experiments, and the final removal rate still reached 93%, which also showed a high removal efficiency for other refractory organic pollutants, such as MO, BBH and PNP, the removal rate can reach more than 89%, reflecting that the ZVI-E-Fenton-PMS process has great potential for application. This advanced oxidation process combining two different radical-based processes provides a simple, efficient and cost-effective method for the removal of refractory organic pollutants from industrial wastewater.

List of abbreviations

ZVI	Zero-valent iron
PMS	Peroxymonosulfate
GF	Graphite felt
EPR	Electron paramagnetic resonance
AOPs	Advanced oxidation processes
ROS	Reactive oxidation species
HR-AOPs	Hydroxyl radical-based advanced oxidation processes
SR-AOPs	Sulfate radical-based advanced oxidation processes
EAOP	Electrochemical advanced oxidation process
ORR	Oxygen reduction reaction
DET	Direct electron transfer
TOC	Total organic carbon
MB	Methylene blue
MO	Methyl orange
BBH	Berberine hydrochloride
PNP	p-Nitrophenol

Conflicts of interest

There are no conflicts to declare.

References

1 S. Furihata, A. Kasai, K. Hidaka, M. Ikegami, H. Ohnishi and K. Goka, *Environ. Pollut.*, 2019, **251**, 628–638.

2 S. J. Ye, G. M. Zeng, H. P. Wu, J. Liang, C. Zhang, J. Dai, W. P. Xiong, B. Song, S. H. Wu and J. F. Yu, *Resour., Conserv. Recycl.*, 2019, **140**, 278–285.

3 V. Katheresan, J. Kansedo and S. Y. Lau, *J. Environ. Chem. Eng.*, 2018, **6**, 4676–4697.

4 R. Soury, M. Jabli, T. A. Saleh, W. S. Abdul-Hassan, E. Saint-Aman, F. Loiseau, C. Philouze and H. Nasri, *RSC Adv.*, 2018, **8**, 20143–20156.

5 M. Al-Yaari, T. A. Saleh and O. Saber, *RSC Adv.*, 2021, **11**, 380–389.

6 T. A. Saleh, *Environ. Technol. Innovation*, 2021, **24**, 101821.

7 F. J. Benitez, J. L. Acero, F. J. Real, G. Roldan and F. Casas, *Chem. Eng. J.*, 2011, **168**, 1149–1156.

8 S. J. Ye, G. M. Zeng, X. F. Tan, H. P. Wu, J. Liang, B. Song, N. Tang, P. Zhang, Y. Y. Yang, Q. Chen and X. P. Li, *Appl. Catal., B*, 2020, **269**, 118850.

9 D. H. He, C. Zhang, G. M. Zeng, Y. Yang, D. L. Huang, L. L. Wang and H. Wang, *Appl. Catal., B*, 2019, **258**, 117957.

10 S. Giannakis, K. Y. A. Lin and F. Ghanbari, *Chem. Eng. J.*, 2021, **406**, 127083.

11 J. De Laat, G. T. Le and B. Legube, *Chemosphere*, 2004, **55**, 715–723.

12 S. Figueroa, L. Vazquez and A. Alvarez-Gallegos, *Water Res.*, 2009, **43**, 283–294.

13 D. J. Chen, Y. L. Cheng, N. Zhou, P. Chen, Y. P. Wang, K. Li, S. H. Huo, P. F. Cheng, P. Peng, R. C. Zhang, L. Wang, H. Liu, Y. H. Liu and R. Ruan, *J. Cleaner Prod.*, 2020, **268**, 120694.

14 Y. Yavuz, A. S. Koparal and U. B. Ogutveren, *Desalination*, 2010, **258**, 201–205.

15 C. A. Martinez-Huitle and M. Panizza, *Curr. Opin. Electrochem.*, 2018, **11**, 62–71.

16 C. A. Martinez-Huitle, M. A. Rodrigo, I. Sires and O. Scialdone, *Chem. Rev.*, 2015, **115**, 13362–13407.

17 J. Li, Q. Liu, G. Gou, S. R. Kang, X. Tan, B. Tan, L. G. Li, N. W. Li, C. Liu and B. Lai, *Sep. Purif. Technol.*, 2022, **286**, 120471.

18 L. Wojnarovits and E. Takacs, *Chemosphere*, 2019, **220**, 1014–1032.

19 Q. F. Wang, Y. S. Shao, N. Y. Gao, W. H. Chu, J. X. Chen, X. Lu, Y. P. Zhu and N. An, *Sep. Purif. Technol.*, 2017, **189**, 176–185.

20 W. D. Oh, Z. L. Dong and T. T. Lim, *Appl. Catal., B*, 2016, **194**, 169–201.

21 P. Neta, R. E. Huie and A. B. Ross, *J. Phys. Chem. Ref. Data*, 1988, **17**, 1027–1284.

22 G. V. Buxton, C. L. Greenstock, W. P. Helman and A. B. Ross, *J. Phys. Chem. Ref. Data*, 1988, **17**, 513–886.

23 W. H. Glaze and J.-W. Kang, *J. - Am. Water Works Assoc.*, 1988, **88**, 57–63.

24 X. J. Chen, X. M. Hu and Y. Gao, *Chem. Eng. J.*, 2019, **359**, 419–427.

25 P. D. Hu and M. C. Long, *Appl. Catal., B*, 2016, **181**, 103–117.

26 R. Y. Xiao, Z. H. Luo, Z. S. Wei, S. Luo, R. Spinney, W. C. Yang and D. D. Dionysiou, *Curr. Opin. Chem. Eng.*, 2018, **19**, 51–58.

27 S. J. Yang, X. J. Qiu, P. K. Jin, M. Dzakpasu, X. C. C. Wang, Q. H. Zhang, L. Zhang, L. Yang, D. H. Ding, W. D. Wang and K. Wu, *Chem. Eng. J.*, 2018, **353**, 329–339.

28 J. L. Wang and L. J. Xu, *Crit. Rev. Environ. Sci. Technol.*, 2012, **42**, 251–325.

29 W. Q. Wang, M. Chen, D. B. Wang, M. Yan and Z. F. Liu, *Sci. Total Environ.*, 2021, **772**, 145522.

30 M. Nashat, M. Mossad, H. K. El-Etriby and M. G. Alalm, *Chemosphere*, 2022, **286**, 131579.

31 F. Ghanbari and C. A. Martinez-Huitle, *J. Electroanal. Chem.*, 2019, **847**, 113182–113182.

32 H. E. Kim, J. Lee, H. Lee and C. Lee, *Appl. Catal., B*, 2012, **115**, 219–224.

33 J. X. Wu, B. Wang, G. Cagnetta, J. Huang, Y. J. Wang, S. B. Deng and G. Yu, *Sep. Purif. Technol.*, 2020, **239**, 116534.

34 W. M. Xiang, Q. Y. Ji, C. M. Xu, Y. Guo, Y. Z. Liu, D. Y. Sun, W. W. Zhou, Z. Xu, C. D. Qi, S. G. Yang, S. Y. Li, C. Sun and H. He, *Appl. Catal., B*, 2021, **285**, 119847.

35 D. B. Song, J. F. Li, Z. Y. Wang and C. Zhao, *Appl. Surf. Sci.*, 2020, **532**, 147450.

36 S. Liu, Z. Y. Wang, J. F. Li, C. Zhao, X. L. He and G. Yang, *Chemosphere*, 2018, **213**, 377–383.

37 X. Han, S. B. Wang, H. W. Huang and Y. H. Zhang, *Appl. Surf. Sci.*, 2021, **540**, 148237.

38 H. Y. Liang, Y. Q. Zhang, S. B. Huang and I. Hussain, *Chem. Eng. J.*, 2013, **218**, 384–391.

39 C. Q. Tan, Y. J. Dong, D. F. Fu, N. Y. Gao, J. X. Ma and X. Y. Liu, *Chem. Eng. J.*, 2018, **334**, 1006–1015.

40 J. Y. Cao, L. D. Lai, B. Lai, G. Yao, X. Chen and L. P. Song, *Chem. Eng. J.*, 2019, **364**, 45–56.

41 L. W. Gao, Y. Guo, J. H. Zhan, G. Yu and Y. J. Wang, *Water Res.*, 2022, **221**, 118730.

42 P. Liang, C. Zhang, X. G. Duan, H. Q. Sun, S. M. Liu, M. O. Tade and S. B. Wang, *Environ. Sci.: Nano*, 2017, **4**, 315–324.

43 X. J. Chen, Y. X. Han, P. Gao and H. Li, *Sep. Purif. Technol.*, 2021, **274**, 118817.

44 J. Lee, U. von Gunten and J. H. Kim, *Environ. Sci. Technol.*, 2020, **54**, 3064–3081.

45 S. D. Yan, W. H. Xiong, S. Y. Xing, Y. Q. Shao, R. Guo and H. Zhang, *Sci. Total Environ.*, 2017, **599**, 1181–1190.

46 S. D. Yan, J. Y. Geng, R. Guo, Y. Du and H. Zhang, *J. Hazard. Mater.*, 2017, **333**, 358–368.

47 N. C. Zheng, X. He, R. T. Hu, R. L. Wang, Q. Zhou, Y. K. Lian and Z. F. Hu, *Appl. Catal., B*, 2022, **307**, 121157.

48 Z. Liu, H. J. Ding, C. Zhao, T. Wang, P. Wang and D. D. Dionysiou, *Water Res.*, 2019, **159**, 111–121.